Chapter 2
On the Size Effects in Indentation Testing of Elastic Functionally-graded Materials

Ivan Argatov

Abstract The size effect in the small-scale indentation testing is studied for a functionally-graded material (FGM) whose shear elastic modulus varies according to the exponential law. Under the simplifying assumption of zero Poisson's ratio, the asymptotic model of the indentation stiffness for an axisymmetric frictionless indenter is developed in the case when the contact radius is small compared to the inhomogeneity characteristic size. The so-called sample size effect is considered on the example of a simply supported FGM plate indented at the center of its top surface. A certain range of applicability of the first-order asymptotic models has been established by comparison with the approximate analytical solution available in the literature.

Keywords: Indentation stiffness · Functionally graded material · Size effect · Asymptotic model

2.1 Introduction

Indentation techniques represent a simple practical method of nondestructive characterizing mechanical properties of materials, e.g., hardness (Oliver and Pharr, 1992), elastic modulus (Bulychev et al, 1975), plasticity (Müller et al, 2009), fracture toughness (Anstis et al, 1981), adhesion strength (Borodich and Galanov, 2008). For instance, when the thermo-mechanical properties of micromechanical components (e.g., of solder joints, are to be determined realistically from small test volumes) a microindentation technique can be utilized (Villain et al, 2008), as it allows to measure the mechanical properties locally in the material.

Ivan Argatov
Department of Materials Science and Applied Mathematics, Malmö University, SE-205 06 Malmö, Sweden,
e-mail: ivan.argatov@gmail.com

B. E. Abali et al. (eds.), *New Achievements in Continuum Mechanics and Thermodynamics*, Advanced Structured Materials 108,
https://doi.org/10.1007/978-3-030-13307-8_2

An indentation test can be performed with a rigid indenter whose displacement, δ, can be monitored under an externally applied contact load, F, and an appropriate mathematical material model is needed to extract the material parameters from the indentation data. Generally speaking, a complete stress-strain curve should be determined for a full characterization of the elastic-plastic deformation behavior (Müller et al, 2009).

With the development of the Oliver–Pharr method (Oliver and Pharr, 1992), nanoindentation, known as an instrumented indentation test, where the direct inspection of the indent imprint is replaced by an indirect assessment from the force-displacement curve, has emerged as an indispensable technique for evaluation of mechanical properties at micro- and nano-scales (Borodich and Keer, 2004; Argatov, 2010). However, practical application of the nanoindentation method can be accompanied with numerous technological difficulties, especially, if a tested material exhibits a fine microstructure (Albrecht et al, 2005; Gibson, 2014; Argatov and Sabina, 2017) and/or a complicated deformation behavior (Cheng et al, 2000; Koumi et al, 2014). In response to the continuous miniaturization of microelectronic components in modern electronic industry, a number of practically important issues in indentation testing have been resolved by the research group headed by Prof. W.H. Müller (TU Berlin).

In particular, essential for the correct determination of the contact area in the depth-sensing indentation is the precise measurement of the actual indentation depth of the indenter. This practical issue has been addressed by Müller et al (2011). The evaluation of the material properties at elevated temperature reveals the influence of the surface oxidation on the indentation data. To avoid this problem, Müller et al (2009) developed an effective measurement procedure, which is of particular significance for characterizing the solder materials. The effect of crystal grain orientation is another parameter, which influences the accuracy of detailed indentation analysis of local material properties, was studied by Müller et al (2009). For describing the time-dependence of material response shown by low melting solder materials, which under indentation load are susceptible to creep behavior, Müller and Worrack (2012) have developed an enhanced analysis of nanoindentation data based on rheological models. To obtain information on the material's work hardening from experimentally measured load-displacement curves obtained with a blunt probe, the inverse analysis based determination methodology was established by Weinberg et al (2005). A practically important problem arises in application of nanoindentation for determining the mechanical properties of individual phases in heterogeneous materials and, especially, of intermetallic phases in microelectronic structures. It has been shown (Albrecht et al, 2005) that nanoindentation can be effectively used to quantify the growth of intermetallic phases, in particular at the interface of a solder connection.

What interests us in nanoindentation is that in many cases the effect of plastic deformations on the elastic deformation response can be get rid of by considering the indentation unloading (Bulychev et al, 1975), so that by evaluating the incremental indentation stiffness

$$S = \frac{\mathrm{d}F}{\mathrm{d}\delta}, \tag{2.1}$$

one can assess the stiffness property of solid materials, which for an isotropic homogeneous linearly elastic material, is fully characterized by its shear modulus, G, and Poisson's ratio, ν.

In the case of an axisymmetric indenter (e.g., cylinder, sphere, or cone), the evaluation of elastic indentation test is based on the BASh (Bulychev–Alekhin–Shorshorov) relation (Bulychev et al, 1975)

$$S(a) = \frac{4aG}{1-\nu}, \tag{2.2}$$

which reveals the fact that the indentation stiffness is proportional to the radius of contact area, a.

Equations (2.1) and (2.2) show that the ratio $S(a)/\sqrt{A}$, where A is the contact area, should be insensitive to the size of the indenter imprint. However, for a functionally-graded material, when, in addition to its elastic moduli, the material's response to indentation depends on some characteristic size of material inhomogeneity, the ratio $S(a)/a$ (in the axisymmetric setting) will vary with the contact radius a, thereby exhibiting the size effect. This issue was considered using either experimental, analytical or numerical methods (e.g., Suresh et al, 1997; Gouldstone et al, 2007).

Recall (Markworth et al, 1995) that the concept of functionally graded material (FGM) refers to composite materials with spatially variable properties, which is usually achieved by gradual compositional variation of the constituents. The development of indentation methods for a FGM sample requires the solution of contact problems for a semi-infinite elastic medium with a continuous variation of elastic properties (e.g., Giannakopoulos and Suresh, 1997b; Aizikovich et al, 2002; Heß, 2016; Argatov et al, 2018). Moreover, in order to assess the sample size effect, the corresponding contact problem should be formulated for a finite body, and such problems still remain to be solved by analytical methods.

Recently, the three-dimensional elastic deformation of an isotropic functionally graded plate subjected to point loading was solved by Abali et al (2014) in the special case of exponentially graded inhomogeneity using the analytical approach based on the displacement functions method (Plevako, 1971; Kashtalyan, 2004). In the present paper, we make use of the obtained singular solution and employ asymptotic modeling approach (Argatov, 2010) for evaluating the local indentation stiffness of a simply supported FGM plate in the range of small-scale indentation.

2.2 Small-scale Indentation

To fix our ideas, we consider indentation of a FGM sample, which is supposed to be isotropic with a constant Poisson's ratio, ν. To be more precise, we assume that the shear elastic modulus, $G(x_3)$, varies according to an exponential law of the type

$$G(x_3) = G_0 \exp\Big(\frac{x_3}{l}\Big), \tag{2.3}$$

where G_0 is the value of the shear modulus at the surface, x_3 is a Cartesian coordinate measured along the inner normal to the indented surface $x_3 = 0$, and l is the characteristic size of inhomogeneity.

In the general case of in-depth functionally graded material, the inhomogeneity characteristic size can be introduced as follows:

$$l = \left|\frac{G(0)}{G'(0)}\right|. \tag{2.4}$$

Here, $G'(0)$ is the right-hand derivative of the function $G(x_3)$ at $x_3 = 0$.

Let a be a characteristic size of the contact area, e.g., the contact radius in the case of axisymmetric indenter and a circular contact area. Then, the range of small-scale indentation can be characterized by assuming that $a/l \ll 1$. An approximate solution of the contact problem for a frictionless cylindrical indenter (Fig. 2.1) and an exponentially graded elastic medium (2.3) in the special case $\nu = 0$ was obtained by Giannakopoulos and Suresh (1997b). Based on their results, the indentation stiffness can be evaluated as follows:

$$S(a) \approx 4aG_0\left\{1 - \frac{2}{\pi}\frac{a}{l}\left(C_0 - \frac{C_1}{3}\Big(\frac{a}{l}\Big)^3 + \frac{2C_1^2}{45\pi}\Big(\frac{a}{l}\Big)^5\right)\right\}^{-1}. \tag{2.5}$$

Here, $C_0 = 3.7$ and $C_1 = 403.5$.

Observe that the factor $4aG_0$, which stands just before the curly braces in (2.5), corresponds to the isotropic homogeneous case with the surface shear modulus G_0. It is interesting that the relative difference between $S(a)$, as it is given by (2.5), and $4aG_0$ is less than 5% only in a relatively small interval $[0, 0.02)$. At the same time, the 5 percent interval for the first order approximation $S(a) \approx 4aG_0\{1 - (2/\pi)C_0(a/l)\}$ is longer and equal to $[0, 0.16)$. This example shows that due to the size effect, the classical BASh formula (2.2) and the Oliver–Pharr method can be applied only in a limited contact size range.

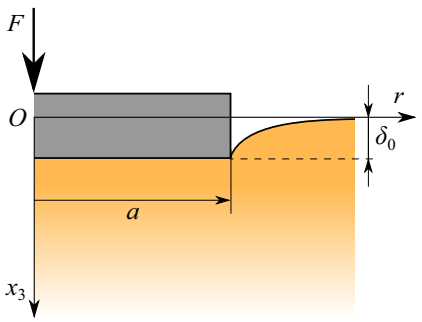

Fig. 2.1 Schematic of the cylindrical flat-ended indentation

2.3 First-order Asymptotic Model for the Indentation Stiffness

Let $G_3(x_1, x_2)$ denote the surface influence function in the Boussinesq problem of acting a unit point force on the surface of an elastic half-space along the normal to the surface and directed inside the half-space. In the case of exponentially graded material (2.3) with zero Poisson's ratio, the following solution holds (Giannakopoulos and Suresh, 1997a):

$$G_3(r) = \frac{1}{2\pi G_0 l} \int_0^\infty \mathcal{L}(u) J_0\Big(\frac{r}{l}u\Big)\,\mathrm{d}u. \tag{2.6}$$

Here, $r = \sqrt{x_1^2 + x_2^2}$ is a polar radius, $J_0(t)$ is the zeroth order Bessel function of the first kind, and

$$\mathcal{L}(u) = \frac{2u\sqrt{(2u)^2+1}}{\big(1+\sqrt{(2u)^2+1}\big)^2}. \tag{2.7}$$

First of all we observe that

$$\mathcal{L}(u) = 1 + D_1 u^{-1} + O(u^{-2}), \quad u \to \infty, \tag{2.8}$$

with $D_1 = -1$ and, therefore, the integral in (2.6) diverges as $r \to 0$.

To proceed, we recall the known formulas (e.g., Gradshteyn and Ryzhik, 1994, formulas (6.511.1) and (6.532.4))

$$\int_0^\infty J_0(ut)\,\mathrm{d}u = \frac{1}{t}, \quad \int_0^\infty \frac{uJ_0(ut)}{u^2+1}\,\mathrm{d}u = K_0(t), \tag{2.9}$$

where $K_0(t)$ is the Macdonald function, which admits the asymptotic expansion

$$K_0(t) = -\ln\frac{t}{2} + \gamma + O(t^2), \quad t \to 0, \tag{2.10}$$

with $\gamma = 0.557\ldots$ being Euler's constant.

Now, by accounting for (2.9) and (2.10), it can be shown that the integral in Eq. (2.6) possesses the asymptotic expansion

$$\int_0^\infty \mathcal{L}(u) J_0\Big(\frac{r}{l}u\Big)\,\mathrm{d}u = \frac{l}{r} + D_1 \ln\frac{l}{r} - a_0 + O\Big(\frac{r}{l}\Big), \quad r \to 0, \tag{2.11}$$

where $D_1 = -1$ is the asymptotic constant in (2.8) and a_0 is given by

$$a_0 = -D_1(\ln 2 - \gamma) + \int_0^\infty \Big(1 - \mathcal{L}(u) + \frac{D_1 u}{u^2+1}\Big)\mathrm{d}u. \tag{2.12}$$

Thus, in light of (2.11), we obtain

$$G_3(r) = \frac{1}{2\pi G_0}\left(\frac{1}{r} + \frac{D_1}{l}\ln\frac{l}{r} - \frac{a_0}{l} + O\Big(\frac{r}{l}\Big)\right), \quad r \to 0. \tag{2.13}$$

In order to determine the indentation stiffness, we consider the frictionless indentation problem for a flat-ended cylindrical indenter of radius a, which can be formulated in the form of the following integral equation (Vorovich et al, 1974):

$$\int_0^a p(\bar{r})K\Big(\frac{\bar{r}}{l}, \frac{r}{l}\Big)\bar{r}\,\mathrm{d}\bar{r} = \theta_0 l\delta_0. \tag{2.14}$$

Here, $p(r)$ is the contact pressure, $\theta_0 = G_0/(1-\nu)$ is an elastic constant, δ_0 is the indenter displacement, and the kernel $K(s,t)$ is given by the integral

$$K(s,t) = \int_0^\infty \mathcal{L}(u)J_0(us)J_0(ut)\,\mathrm{d}u.$$

It can be shown (e.g., Vorovich et al, 1974) that the solution of Eq. (2.14) is related to the solution $q(r)$ of the integral equation

$$\int_0^a q(\bar{x})\,\mathrm{d}\bar{x}\int_0^\infty \mathcal{L}(u)\cos\frac{\bar{x}}{l}u\cos\frac{x}{l}u\,\mathrm{d}u = \frac{\pi}{2}\theta_0 l\delta_0 \tag{2.15}$$

via the formula

$$p(r) = \frac{2}{\pi}\left(\frac{q(a)}{\sqrt{a^2-r^2}} - \int_r^a \frac{q'(\bar{r})\,\mathrm{d}\bar{r}}{\sqrt{\bar{r}^2-r^2}}\right). \tag{2.16}$$

In turn, by introducing the dimensionless variables

$$\varphi(\xi) = \frac{q(\xi a)}{\theta_0 a}, \quad \xi = \frac{x}{a}, \quad \lambda = \frac{l}{a}, \quad f_0 = \frac{\delta_0}{a}, \tag{2.17}$$

the integral equation (2.15) can be transformed to the following form (Vorovich et al, 1974):

$$\varphi(\xi) - \frac{1}{\pi\lambda}\int_{-1}^1 \varphi(\bar{\xi})k\Big(\frac{\xi-\bar{\xi}}{\lambda}\Big)\,\mathrm{d}\bar{\xi} = f_0. \tag{2.18}$$

Here we have introduced the notation

$$k(t) = \int_0^\infty \big[1-\mathcal{L}(u)\big]\cos ut\,\mathrm{d}u. \tag{2.19}$$

Further, for the function $\mathcal{L}(u)$ given by Eq. (2.7) and satisfying the asymptotic expansion (2.8), it can be verified that the following expansion holds (Ajzikovich and Aleksandrov, 1986):

$$k(t) = D_1 \ln|t| - a_{30} + O(t), \quad t \to 0. \tag{2.20}$$

The asymptotic constant a_{30} is given by (cf. Eq. (2.12))

$$a_{30} = \int_0^\infty \left(\mathcal{L}(u) - 1 - \frac{D_1(1 - e^{-u})}{u} \right) \mathrm{d}u. \tag{2.21}$$

Using the properties of the digamma function, we find

$$a_{30} = -a_0 - D_1 \ln 2, \tag{2.22}$$

where a_0 is the asymptotic constant (2.12).

Finally, substituting the asymptotic approximation (2.20) into Eq. (2.18) and assuming that $\lambda \gg 1$, we readily find the first-order asymptotic approximation of its solution in the form

$$\varphi(\xi) \simeq f_0 \left\{ 1 + \frac{1}{\pi\lambda} \int_{-1}^{1} \left(D_1 \ln \frac{|\xi - \bar{\xi}|}{\lambda} - a_{30} \right) \mathrm{d}\bar{\xi} \right\}. \tag{2.23}$$

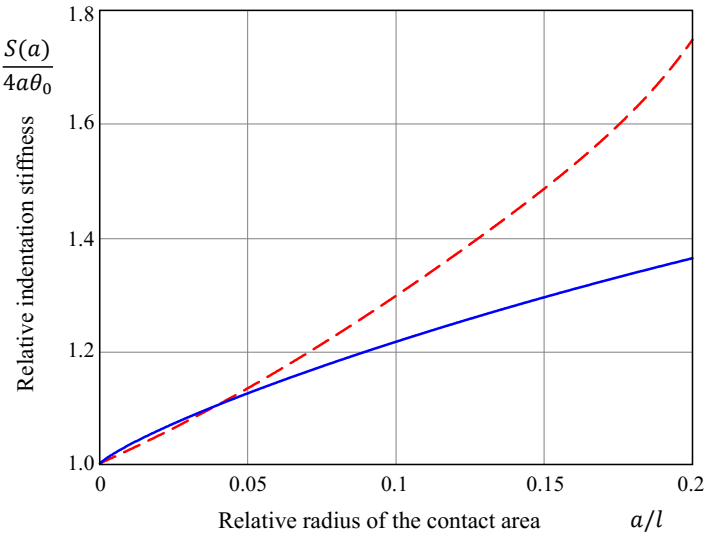

Fig. 2.2 Predictions for the relative indentation stiffness according to the approximate formula (2.5) (dashed line) and the asymptotic formula (2.25) (solid line)

By direct integration, it can be shown that

$$\int_{-1}^{1} \ln \frac{1}{|\xi - \bar{\xi}|} \, \mathrm{d}\bar{\xi} = -\ln(1-\xi^2) + 2 + \xi \ln\Big(\frac{1-\xi}{1+\xi}\Big).$$

Thus, the substitution of (2.23) into Eqs. (2.16) and (2.17) yields

$$p(r) \simeq \frac{2}{\pi} \frac{\theta_0 \delta_0}{a} \left\{ \frac{1}{\sqrt{1-\rho^2}} \left(1 - \frac{1}{\pi\lambda} \left[2D_1 \Big(1 + \ln \frac{\lambda}{2} \Big) - 2a_{30} \right] \right) + \frac{D_1}{\pi\lambda} \int_{\rho}^{1} \ln\left(\frac{1-\xi}{1+\xi} \right) \frac{\mathrm{d}\xi}{\sqrt{\xi^2 - \rho^2}} \right\}, \tag{2.24}$$

where $\rho = r/a$ is the dimensionless polar radius.

In turn, the substitution of (2.24) into the formula

$$S(a) = \frac{2\pi}{\delta_0} \int_0^a p(r) r \, \mathrm{d}r$$

leads to the following first-order asymptotic model for the indentation stiffness (cf. Ajzikovich and Aleksandrov, 1986)

$$S(a) \simeq 4a\theta_0 \left\{ 1 + \frac{1}{\pi\lambda} \left(D_1 \Big(3 + 2 \ln \frac{\lambda}{2} \Big) + 2a_{30} \right) \right\}^{-1}. \tag{2.25}$$

Here, λ is the large dimensionless parameter given by (2.17).

Note that the relative difference between the asymptotic solution (2.25) and the approximate solution (2.5) does not exceed 5% in the interval $[0, 0.09)$. It should be emphasized that the expression on the right-hand side of (2.5) has a singularity for a certain value of the ratio a/l. Hence, the accuracy of the approximate solution (2.5) is doubtful for small values of λ, where the asymptotic solution (2.25) fails as well.

2.4 Sample Size Effect in Indentation of a FGM Plate

It is clear that formulas (2.5) and (2.25) can be applied when, in addition, the contact radius a is much smaller than the sample's characteristic size, h. Moreover, in the case of a tested sample of finite size, the clamping conditions should be accounted for as well. To illustrate this issue, we consider the problem of indentation of a square FGM plate, which is assumed to be simply supported at its perimeter. In order to construct an asymptotic model for the indentation stiffness, we need the singular solution of the boundary-value problem of point loading of the plate (see

Fig. 2.3), which was investigated by a combination of analytical and numerical tools by Abali et al (2014).

Let the plate be referred to a Cartesian coordinate system (x_1, x_2, x_3), so that $-b/2 \le x_1 \le b/2$, $-b/2 \le x_2 \le b/2$, $0 \le x_3 \le h$. Let us also introduce the new vertical variable

$$z = h - x_3, \tag{2.26}$$

which has been used in the analysis of Abali et al (2014) and Kashtalyan (2004). According to Plevako's general solution (Plevako, 1971), the vertical component of the displacement vector can be represented in the following form (Kashtalyan, 2004)

$$\mathcal{G}_3(\mathbf{x}) = \frac{1}{G}\sum_{m=1}^{\infty}\sum_{n=1}^{\infty}\Bigg\{-(1-\nu)\left(\frac{1}{l}\frac{\partial^2 L_{mn}}{\partial z^2}(\mathbf{x}) + \frac{\partial^3 L_{mn}}{\partial z^3}(\mathbf{x})\right) + \alpha_{mn}^2\left((2-\nu)\frac{\partial L_{mn}}{\partial z}(\mathbf{x}) - \frac{\nu}{l}L_{mn}(\mathbf{x})\right)\Bigg\}. \tag{2.27}$$

Here we have introduced the notation

$$L_{mn}(\mathbf{x}) = \phi_{mn}(z)\sin\frac{\pi m}{b}\left(\frac{b}{2}+x_1\right)\sin\frac{\pi m}{b}\left(\frac{b}{2}+x_2\right), \tag{2.28}$$

$$\phi_{mn}(z) = h^4\left[A_{1mn}f_{1mn}(z) + A_{2mn}f_{2mn}(z) + A_{3mn}f_{3mn}(z) + A_{4mn}f_{4mn}(z)\right],$$

$$f_{1mn}(z) = e^{-z/l}\cosh\frac{\lambda_{mn}z}{h}\cos\frac{\mu_{mn}z}{h},\ f_{2mn}(z) = e^{-z/l}\sinh\frac{\lambda_{mn}z}{h}\cos\frac{\mu_{mn}z}{h},$$

$$f_{3mn}(z) = e^{-z/l}\cosh\frac{\lambda_{mn}z}{h}\sin\frac{\mu_{mn}z}{h},\ f_{4mn}(z) = e^{-z/l}\sinh\frac{\lambda_{mn}z}{h}\sin\frac{\mu_{mn}z}{h}.$$

The constants A_{1mn}, A_{2mn}, A_{3mn}, and A_{4mn} can be found from the boundary conditions on the top and bottom surfaces of the plate, λ_{mn} and μ_{mn} are the roots of the characteristic equations (see Abali et al, 2014; Kashtalyan, 2004, for details), and $\alpha_{mn} = \pi\sqrt{m^2+n^2}/b$. In the case of unit point loading, we have

$$\sigma_{33}\big|_{x_3=0} = -\frac{4}{b^2}\sum_m\sum_n \cos\frac{\pi m}{b}x_1\cos\frac{\pi m}{b}x_2, \tag{2.29}$$

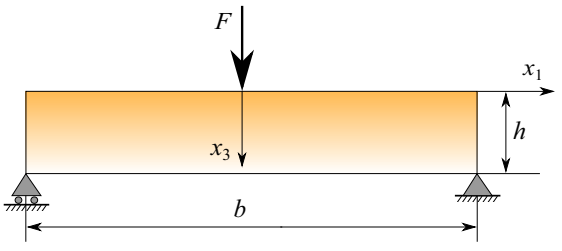

Fig. 2.3 Schematic of the point loading of a square simply supported FGM plate

where $m, n = 1, 3, 5, \ldots$.

Thus, in view of Eqs. (2.27)–(2.29), the surface normal displacement of the FGM plate can be represented in the form

$$\mathcal{G}_3(x_1, x_2, 0) = \frac{1}{2\pi G_0 l} \sum_m \sum_n \mathcal{A}_{mn} \cos\frac{\pi m}{b} x_1 \cos\frac{\pi m}{b} x_2, \tag{2.30}$$

where the dimensionless coefficients $\mathcal{A}_{mn}$ are linear combinations of A_{1mn}, A_{2mn}, A_{3mn}, and A_{4mn} $(m, n = 1, 3, 5, \ldots)$.

For a FGM plate of the type (2.6), it can be shown that the singular function (2.30) satisfies the asymptotic expansion of the type (2.13). In light of this fact, we introduce the notation

$$\mathcal{B}^{(1)}_{mn} = \frac{16l}{b^2} \int_0^{b/2} \int_0^{b/2} \frac{1}{\sqrt{x_1^2 + x_2^2}} \cos\frac{\pi m}{b} x_1 \cos\frac{\pi m}{b} x_2 \, \mathrm{d}x_1 \mathrm{d}x_2, \tag{2.31}$$

$$\mathcal{B}^{(2)}_{mn} = \frac{16}{b^2} \int_0^{b/2} \int_0^{b/2} \ln\frac{l}{\sqrt{x_1^2 + x_2^2}} \cos\frac{\pi m}{b} x_1 \cos\frac{\pi m}{b} x_2 \, \mathrm{d}x_1 \mathrm{d}x_2, \tag{2.32}$$

and put

$$\mathcal{A}_0 = -\left(2\pi G_0 l \mathcal{G}_3(x_1, x_2, 0) - \frac{l}{r} + D_1 \ln\frac{l}{r} \right)\Bigg|_{r=0}, \tag{2.33}$$

where $D_1 = -1$ is the asymptotic constant from the asymptotic expansion (2.13) for the fundamental solution $G_3(r)$ of the Boussinesq problem for a FGM half-space.

Then, according to (2.30)–(2.33), we find

$$\mathcal{A}_0 = -\sum_m \sum_n \left(\mathcal{A}_{mn} - \mathcal{B}^{(1)}_{mn} - D_1 \mathcal{B}^{(2)}_{mn} \right). \tag{2.34}$$

Finally, by applying the asymptotic modeling approach (Argatov, 2010) it can be shown that the first order model for the indentation stiffness is given by

$$S(a) \approx 4a\theta_0 \left\{ 1 + \frac{1}{\pi\lambda} \left(D_1 \left(3 + 2\ln\frac{\lambda}{2} \right) + 2\mathcal{A}_{30} \right) \right\}^{-1}, \tag{2.35}$$

where, in view of (2.22), we have

$$\mathcal{A}_{30} = -\mathcal{A}_0 - D_1 \ln 2$$

with $\mathcal{A}_0$ being given by (2.34), and $\lambda = l/a$ is the dimensionless parameter introduced by (2.17), which is expected to take large values.

Observe that the asymptotic model (2.35) requires that the characteristic inhomogeneity length l should be smaller than the sample thickness h, so that $a \ll h$, as well as $a \ll b$, where a is the contact radius and b is the plate width.

2.5 Discussion and Conclusion

It should be emphasized that asymptotic models, which are usually derived under certain simplifying assumptions, should not be exploited outside the range of their applicability. With regard to the asymptotic models developed above, we observe that the singular solution (2.6), (2.5) was obtained in the special case where $\nu = 0$. For the more realistic case of non-zero Poisson's ratio, the factor $(2\pi G_0)^{-1}$ in (2.6) should be replaced with $(1-\nu)/(2\pi G_0)$, and, apparently, the asymptotic constant D_1 in (2.8) will be a function of ν.

In the general case of a functionally graded material with constant Poisson's ratio, the first-order asymptotic model (2.25) still can be used, provided the inhomogeneity characteristic size l is defined by formula (2.4).

It should be noted that the 5 percent interval, determined for the asymptotic model (2.25) based on the approximate solution (2.5) is rather small (see Fig. 2.2). This, in particular, implies that further research is needed to understand the strength of the size effect.

References

Abali BE, Völlmecke C, Woodward B, Kashtalyan M, Guz I, Müller WH (2014) Three-dimensional elastic deformation of functionally graded isotropic plates under point loading. Composite Structures 118:367–376

Aizikovich SM, Alexandrov VM, Kalker JJ, Krenev LI, Trubchik IS (2002) Analytical solution of the spherical indentation problem for a half-space with gradients with the depth elastic properties. International Journal of Solids and Structures 39(10):2745–2772

Ajzikovich SM, Aleksandrov VM (1986) Asymptotic solutions to contact problems of elasticity theory for half-space and half-plane inhomogeneous by depth (in Russ.). Izvestiya AN Armjanskoj SSR Mehanika 3:13–28

Albrecht HJ, Hannach T, Häse A, Juritza A, Müller K, Müller WH (2005) Nanoindentation: a suitable tool to determine local mechanical properties in microelectronic packages and materials? Archive of Applied Mechanics 74(11):728–738

Anstis GR, Chantikul P, Lawn BR, Marshall DB (1981) A critical evaluation of indentation techniques for measuring fracture toughness: I. Direct crack measurements. Journal of the American Ceramic Society 64(9):533–538

Argatov I (2010) Frictionless and adhesive nanoindentation: Asymptotic modeling of size effects. Mechanics of Materials 42(8):807–815

Argatov I, Sabina F (2017) A two-phase self-consistent model for the grid indentation testing of composite materials. International Journal of Engineering Science 121:52–59

Argatov I, Heß M, Popov VL (2018) The extension of the method of dimensionality reduction to layered elastic media. ZAMM - Journal of Applied Mathematics and Mechanics / Zeitschrift für Angewandte Mathematik und Mechanik 98(4):622–634

Borodich FM, Galanov BA (2008) Non-direct estimations of adhesive and elastic properties of materials by depth-sensing indentation. Proceedings: Mathematical, Physical and Engineering Sciences (The Royal Society) 464(2098):2759–2776

Borodich FM, Keer LM (2004) Contact problems and depth-sensing nanoindentation for frictionless and frictional boundary conditions. International Journal of Solids and Structures 41(9):2479–2499

Bulychev SI, Alekhin VP, Shorshorov MK, Ternovskij AP, Shnyrev GD (1975) Determination of young modulus by the hardness indentation diagram (in Russ. Zavodskaya Laboratoriya 41(9):1137–1140

Cheng L, Xia X, Yu W, Scriven LE, Gerberich WW (2000) Flat-punch indentation of viscoelastic material. Journal of Polymer Science Part B: Polymer Physics 38(1):10–22

Giannakopoulos AE, Suresh S (1997a) Indentation of solids with gradients in elastic properties: Part I. Point force. International Journal of Solids and Structures 34(19):2357–2392

Giannakopoulos AE, Suresh S (1997b) Indentation of solids with gradients in elastic properties: Part II. Axisymmetric indentors. International Journal of Solids and Structures 34(19):2393–2428

Gibson RF (2014) A review of recent research on nanoindentation of polymer composites and their constituents. Composites Science and Technology 105:51–65

Gouldstone A, Chollacoop N, Dao M, Li J, Minor AM, Shen YL (2007) Indentation across size scales and disciplines: Recent developments in experimentation and modeling. Acta Materialia 55(12):4015–4039

Gradshteyn IS, Ryzhik IM (1994) Tables of Integrals, Series and Products. Academic Press, New York

Heß M (2016) A simple method for solving adhesive and non-adhesive axisymmetric contact problems of elastically graded materials. International Journal of Engineering Science 104:20–33

Kashtalyan M (2004) Three-dimensional elasticity solution for bending of functionally graded rectangular plates. European Journal of Mechanics - A/Solids 23(5):853–864

Koumi KE, Nelias D, Chaise T, Duval A (2014) Modeling of the contact between a rigid indenter and a heterogeneous viscoelastic material. Mechanics of Materials 77:28–42

Markworth AJ, Ramesh KS, Parks WP (1995) Modelling studies applied to functionally graded materials. Journal of Materials Science 30(9):2183–2193

Müller WH, Worrack H (2012) Analysis of nanoindentation experiments by means of rheological models. PAMM 12(1):293–294

Müller WH, Worrack H, Sterthaus J, Villain J, Wilden J, Juritza A (2009) How to extract continuum materials properties for (lead-free) solders from tensile tests and nanoindentation experiments. Microsystem Technologies 15(1):45–55

Müller WH, Worrack H, Sterthaus J, Wilden J (2009) Nanoindentation experiments at elevated temperatures for the determination of mechanical solder material properties. PAMM 9(1):719–720

Müller WH, Worrack H, Zapara M (2011) Analysis of nanoindentation experiments by means of atomic force microscopy. PAMM 11(1):413–414

Oliver WC, Pharr GM (1992) An improved technique for determining hardness and elastic modulus using load and displacement sensing indentation experiments. Journal of Materials Research 7(6):1564–1583

Plevako VP (1971) On the theory of elasticity of inhomogeneous media. Journal of Applied Mathematics and Mechanics 35(5):806–813

Suresh S, Giannakopoulos AE, Alcalá J (1997) Spherical indentation of compositionally graded materials: Theory and experiments. Acta Materialia 45(4):1307–1321

Villain J, Mueller WH, Haese A, Weippert C, Corradi U, Saeed U (2008) Determination of mechanical properties of small test volumes using nanoindentation - a critical review. In: 2008 2nd Electronics System-Integration Technology Conference, pp 155–162

Vorovich II, Aleksandrov VM, Babeshko VA (1974) Non-Classical Mixed Problems in the Theory of Elasticity (in Russ.). Nauka, Moscow

Weinberg K, Sterthaus J, Müller WH (2005) Determining material parameter of solder alloys by nanoindentation. PAMM 5(1):451–452